June, 1996

LIDS-P 2344

Research Supported By:

German Educational Exchange Service (DAAD)
ARPA contract F30602-92-C-0030

Rate-Distortion Performance for Joint Source and Channel Coding of Images

Ruf, Michael J.
Modestino, James W.

June 1996

LIDS-P-2344

Rate-Distortion Performance for Joint Source and Channel Coding of Images*

Michael J. Ruf
German Aerospace Research Establishment (DLR)
Institute for Communications Technology
D - 82234 Wessling, Germany

James W. Modestino
ECSE Department
Rensselaer Polytechnic Institute
Troy, NY, 12180, U.S.A.

Abstract

This paper describes a methodology for evaluating the rate-distortion behavior of combined source and channel coding schemes with particular application to images. In particular, we demonstrate use of the operational rate-distortion function to obtain the optimum tradeoff between source coding accuracy and channel error protection under the constraint of a fixed transmission bandwidth. Furthermore, we develop information-theoretic bounds on performance and demonstrate that our combined source-channel coding methodology results in rate-distortion performance which closely approach these theoretical limits. We concentrate specifically on a wavelet-based subband source coding scheme and the use of binary rate-compatible punctured convolutional (RCPC) codes for transmission over the additive white Gaussian noise (AWGN) channel. Explicit results for real-world images demonstrate the efficacy of this approach.

1 Introduction

Shannon's information theory has established that, in the limit of large block sizes, source and channel coding can be treated separately and if the rate-distortion function of the encoded source is smaller than the channel capacity, theoretically achievable performance is limited solely by source coding errors. However, it can be observed in real-world systems that, even if the source encoded bit stream is almost statistically independent, the individual bits normally differ in their relative importance or sensitivity, and thus should be protected against channel errors according to their

*This work was performed at the ECSE Dept., Rensselaer Polytechnic Institute, Troy, NY 12180 and was supported by the German Educational Exchange Service (DAAD) as part of the HSP II-program, and in part by ARPA under Contract No. F30602-92-C-0030.; and DAAH04-95-1-0103 (Laboratory for Information and Decision Systems, Massachusetts Institute of Technology).

respective effects on the reconstructed image. In recognization of this fact a number of approaches have been developed for improving the quality of reconstructed images under noisy channel conditions while maintaining a fixed overall transmission bandwidth. These techniques include: a number of source and channel coding strategies with specifically tailored assignment of channel codes to different encoded bit positions [1, 2, 3]; various schemes that combine blocked source data structures and channel coding to limit propagation of channel error effects for variable-length and/or predictive coded data [4, 5]; and source-controlled channel decoding schemes [6] that use residual correlation in the encoded data to improve bit-error performance and hence reconstructed image quality. All of these techniques have been shown to provide some degree of performance improvement in the presence of channel errors.

In this paper, we describe how the quantization errors and the channel error effects contribute to the overall distortion as an explicit function of the number of quantization bits used for the different source data streams and on the specific channel codes employed for operation over an additive white Gaussian noise (AWGN) channel at a specific value of E_s/N_0. This will enable us to develop an approach for jointly distributing source and channel bits in an optimum way. In distinction to the work in [3], where a two-stage bit-allocation, first for source and then for channel bits under the constraint of a common overall rate, was used to find the minimum overall distortion over all possible source rates, we describe an improved process with a single joint bit-allocation. This approach considers both the effects of quantization and channel errors contributing to the distortion in case of a noisy environment and allows a trade-off between quantization noise and channel errors in an optimum way. Furthermore, in order to provide a context for this work, we extend this approach to obtain a series of information-theoretic bounds on the achievable performance of practical combined source-channel coding approaches. This allows direct evaluation of the relative efficacy of different quantization, coding and error protection schemes and, in particular, demonstrates that the approach described here provides performance closely approaching these theoretical limits.

This paper is organized as follows. In Section II, we first give a brief description of the source coder, the statistical properties of the various data streams and the different quantizers used. The derivation of the individual sensitivities of the coded bits, depending on the quantizers and the number of quantization bits, is developed together with a comparison of simulated results in Section III. In Section IV, we briefly discuss the channel coder and we describe an approach for optimizing the rate-distortion performance for the (real-world) transmission systems employed, along with

some simulation results. In Section V, we extend the rate-distortion approach to the development of general information-theoretic bounds and compare different image transmission schemes. Finally, in Section VI we provide a summary and conclusions.

2 Source Coder

2.1 Discrete Wavelet Transform

As in other source coding schemes, the image first undergoes a transformation before quantization to decorrelate the source signal and to make the data more suitable for compression. This could be done by a discrete cosine transform (DCT) [7] or a subband transform (SBT) [8]. Since multiresolution representations, or discrete wavelet transforms (WVT), have been applied very successfully in image coding [9] and have demonstrated superior performance, both subjectively and objectively and for both low and high degrees of compression, we will combine this technique with two different scalar quantization schemes to build a base for optimizing the rate-distortion behavior of the joint source and channel coders.

The basic idea of the discrete wavelet transform is the approximation of a full resolution (r=0) image, denoted $\tilde{A}_0 f$, by its discrete detail representations $\tilde{D}^0_{-1} f$, $\tilde{D}^1_{-1} f$, $\tilde{D}^2_{-1} f$ together with the subimage at resolution $r = 1$, denoted $\tilde{A}_{-1} f$. A subsequent approximation of $\tilde{A}_{-1} f$ by $\tilde{A}_{-2} f$ and $\tilde{D}^0_{-2} f$, $\tilde{D}^1_{-2} f$, $\tilde{D}^2_{-2} f$ can be applied iteratively obtaining the mapping at resolution r

$$\tilde{A}_0 f \mapsto (\tilde{A}_{-r} f, \tilde{D}^0_{-r} f, \tilde{D}^1_{-r} f, \tilde{D}^2_{-r} f, \tilde{D}^0_{-r+1} f, \tilde{D}^1_{-r+1} f, \tilde{D}^2_{-r+1} f, ..., \tilde{D}^0_{-1} f, \tilde{D}^1_{-1} f, \tilde{D}^2_{-1} f) \quad . \qquad (1)$$

Here $\tilde{D}^0_{-r} f$, $\tilde{D}^1_{-r} f$ and $\tilde{D}^2_{-r} f$ are the detail representations of $\tilde{A}_{-r+1} f$ at resolution r and $\tilde{A}_{-r} f$ is the resulting resolution r subimage. This discrete wavelet decomposition is illustrated in Fig. 1.

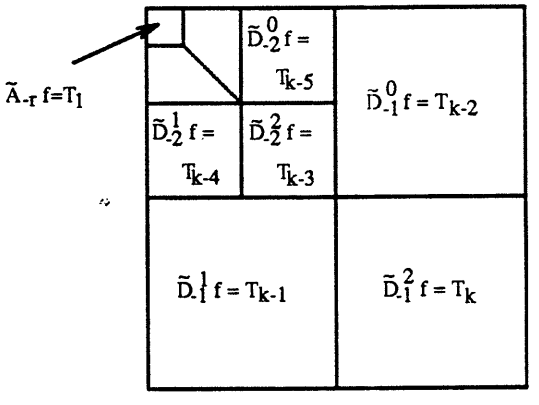

Figure 1: An illustration of the wavelet transformed image.

For images, the discrete representations $\tilde{D}^0_{-r} f$, $\tilde{D}^1_{-r} f$, $\tilde{D}^2_{-r} f$ and the subimage $\tilde{A}_{-r} f$ at res-

olution r can be computed from the subimage $\tilde{A}_{-r+1}f$ at resolution $(r-1)$ by filtering first the rows and then the columns of $\tilde{A}_{-r+1}f$ followed by subsampling by a factor of 2. The discrete representation of the original image at resolution r then consists of $K := 3r+1$ subimages. The two filters $(g_m)_{m\in Z}$ and $(h_m)_{m\in Z}$ which are used to effect the iterative resolution into low and high spatial frequency components, respectively, are related by the condition $g_m = (-1)^{1-m} \cdot h_{1-m}$. Furthermore, wavelet theory shows that $|H(\omega)|^2 - |H(\omega+\pi)|^2 = 2$ for perfect reconstruction, so the filters have the characteristics of quadrature mirror filters (QMFs). Finally, the inverse wavelet transform can be performed by upsampling $\tilde{D}^0_{-r}f$, $\tilde{D}^1_{-r}f$, $\tilde{D}^2_{-r}f$ and $\tilde{A}_{-r}f$ by a factor of 2 and subsequent filtering. In the work reported here, the Johnston 16-tap (b) filter [10] was used for the elementary row and column filtering steps. In the following, let us denote the subimages of the wavelet transformed image matrix T as $T_1 = \tilde{A}_{-r}f$, $T_2 = \tilde{D}^0_{-r}f$, $T_3 = \tilde{D}^1_{-r}f$, $T_4 = \tilde{D}^2_{-r}f$, $T_5 = \tilde{D}^0_{-r+1}f$, etc.

2.2 Statistical Properties of the Source Coders

It has been shown [4] that the histograms of the various subimages can be modeled reasonably accurately in terms of the generalized Gaussian (GG) distribution

$$p(x) = \frac{\beta}{2\alpha\Gamma(1/\beta)} \cdot \exp\left\{|x/\alpha|^\beta\right\} \quad , \tag{2}$$

with α a scale parameter and the parameter β controlling the exponential rate of decay. The parameters α, β associated with a particular subimage can be calculated from the corresponding samples $\mathbf{x} = (x_0, x_1, ..., x_{s-1})$ of that subimage, their expectation μ, their first two absolute moments $A_1 = I\!E(|x-\mu|)$ and $A_2 = I\!E(|x-\mu|^2)$ as $\alpha = A_1 \cdot \frac{\Gamma(1/\beta)}{\Gamma(2/\beta)}$, using

$$\beta = \mathrm{F}^{-1}(\frac{A_2}{A_1^2}) \qquad ; \text{with} \quad \mathrm{F}(\beta) = \frac{\Gamma(1/\beta)\cdot\Gamma(3/\beta)}{\Gamma^2(2/\beta)} \quad . \tag{3}$$

Results have shown that all AC[1]-subimages match the GG-model very good, while the DC-subimage does not and thus will be modeled by a Gaussian distribution (i.e., $\alpha = \sqrt{2\sigma^2}$ and $\beta = 2$, with σ^2 the variance of the samples $\mathbf{x}$).

[1] We use a loose notation here, denoting the lowest-frequency band as the DC-subband and all the higher-frequency bands as AC-subbands

2.3 Quantization and Coding

2.3.1 Scheme A: Uniform Threshold (UT) Quantizer

In this very basic and very fast quantization scheme, the range Q of the samples[2] of the subimage is divided into $N = 2^n$ equally spaced intervals with $x_{t,k}$ $(0 \leq k \leq N)$ the quantization thresholds and n the number of quantization bits per sample. The reconstruction levels will be computed as $x_{l,k} = (x_{t,k} - x_{t,k+1})/2$. The mean-square error (mse) due to quantization can then be roughly estimated as

$$e_{\mathrm{UT},n} = \frac{1}{12}\left(\frac{Q}{2^n}\right)^2 \quad . \tag{4}$$

2.3.2 Scheme B: Optimum (nonuniform) Generalized Gaussian (GG) Quantizer

In the second scheme, the fact that the histograms of the AC-subimages can be modeled as generalized Gaussian (GG) distributions is used. We follow a procedure described by Roe [11] and applied it to the generalized Gaussian distribution (see Appendix A), to calculate the optimum quantization intervals with nonuniform spacing. Because of symmetry about the origin, the reconstruction levels $x_{l,k}$ for a mean-square error criterion ($\theta = 2$) or a linear distortion measure ($\theta = 1$) can easily be derived as

$$x_{l,k} = \alpha\left[(1+\theta)\cdot \mathrm{P}^{-1}\left(\frac{1}{\beta}\ ,\ \frac{2k+1-N}{N+\kappa_\theta}\right)\right]^{1/\beta} \quad ;\quad \text{for}\quad N/2 \leq k < N\ , \tag{5}$$

with $\mathrm{P}^{-1}(a,x)$ the inverse function of the incomplete Gamma-function $\mathrm{P}(a,x)$. The reconstruction levels for $0 \leq k < N/2$ follow as $x_{l,k} = x_{l,(N-1-k)}$ and the correction term κ_θ for $\theta = 2$ can be evaluated as (see Appendix A)

$$\kappa_2 = \left[\mathrm{P}\left(\frac{1}{\beta}, \frac{1}{3}\cdot\left(\frac{\Gamma(2/\beta)}{\Gamma(1/\beta)}\right)^{\beta}\right)\right]^{-1} - 2\ . \tag{6}$$

The quantization thresholds $x_{t,k}$ can similarly be derived as

$$x_{t,k} = \alpha\left[(1+\theta)\cdot \mathrm{P}^{-1}\left(\frac{1}{\beta}\ ,\ \frac{2k-N}{N+\kappa_\theta}\right)\right]^{1/\beta} \quad ;\text{for}\quad N/2 \leq k \leq N\ , \tag{7}$$

and for $0 \leq k < N/2$ as $x_{t,k} = x_{t,(N-k)}$.

For $N = 2^n$ the number of quantization levels, the expected mse due to quantization can be computed as [12]

$$e_{\mathrm{GG},n} \approx \frac{S_g^3}{3}\cdot\frac{1}{\left(2\left(2^n+\gamma_2\right)\right)^2}\ , \tag{8}$$

[2] Q can easily be derived knowing the statistical properties of the subimages. In particular, we assumed Q as the range that covers the underlying distribution with the probability of 0.999.

with the correction term γ_2 given by

$$\gamma_2 = \frac{1}{2\alpha}\left(\frac{S_g^3\Gamma(1/\beta)}{3\Gamma(3/\beta)}\right)^{1/2} - 1 \ , \tag{9}$$

and

$$S_g = 3^{1/\beta}\cdot\left(\frac{2\alpha\Gamma(1/\beta)}{\beta}\right)^{2/3} \ . \tag{10}$$

2.3.3 Source Coding Rate and Distortion

Knowing the mean-square distortion e_{i,n_i} for each subband $i = 1, 2, ..., K$ ($i = 1$ denoting the DC-subband and $i = K$ denoting the highest-frequency subband), with n_i the number of quantization bits allocated to the i^{th} subband, one can easily calculate the expected distortion of a compressed image, D_{S} (measured as the mean-squared error on a per pixel basis), for every possible allocation of different quantizers per subband as

$$D_{\text{S}} = \sum_{i=1}^{K} D_{\text{S},i} = \sum_{i=1}^{K} \frac{s_i}{S}\cdot e_{i,n_i} \ , \tag{11}$$

with K the number of different subbands after the discrete wavelet transform, S the total number of pixels in the original image and $s_i = S/2^{2r_i}$ the number of samples per subband (r_i denoting the resolution of subband i).

The corresponding source rate R_{S} in source bits per pixel (bpp) can also be calculated as

$$R_{\text{S}} = \frac{1}{S}\cdot\sum_{i=1}^{K} s_i\cdot n_i \ . \tag{12}$$

Equations (11) and (12) can be written as $D_{\text{S}}(\mathbf{n}) = \sum_{i=1}^{K} d_i(n_i)$ and $R_{\text{S}}(\mathbf{n}) = \sum_{i=1}^{K} r_i(n_i)$ for an arbitrary allocation $\mathbf{n} = [n_1, n_2, ..., n_K]$. To optimally choose the vector $\mathbf{n}$, we apply the bit-allocation algorithm of Westerink et al. [13] which will also be used in the later joint source and channel bit allocation. The basic idea is to choose (integer) allocations on the convex hull of the operational rate-distortion function $R(D)$. This is done by repeatedly finding a (neighboring) vector $\mathbf{l}$ to the already known vector $\mathbf{k}$ (starting with $\mathbf{k} = [0, 0, ..., 0]$) by solving

$$\sum_{i=1}^{K}\left([r_i(n_i) - r_i(k_i)] - S(\mathbf{l},\mathbf{k})\,[d_i(n_i) - d_i(k_i)]\right) \geq 0 \ , \tag{13}$$

for every possible allocation vector $\mathbf{n}$, with

$$S(\mathbf{l},\mathbf{k}) = \frac{R(\mathbf{l}) - R(\mathbf{k})}{D(\mathbf{l}) - D(\mathbf{k})} \ , \tag{14}$$

the slope of a line on the convex hull for a (new) neighbor allocation vector $\mathbf{l}$ to the already known allocation vector $\mathbf{k}$. Though the solution of (13) normally yields 2 results, we choose the one with the smaller distortion (i.e., $d_i(l_i) - d_i(k_i) < 0$). The iteration is stopped when the allocated bit rate reaches the target bit rate (or if a desired distortion is reached). An example of the resulting bit-allocation is shown in Table 1 for the case of $K = 16$ subbands, the GG-quantizer and a total rate of $R_s = 1.0$ bit per pixel, which leads to a mean-square error of D_S=20.419.

Result of the Bit-allocation				
subband i	variance i	n_i	e_{i,n_i}	$(s_i/S) \cdot e_{i,n_i}$
1	1678498	12	0.324	0.0003
2	198927	10	0.550	0.0005
3	41472	9	1.042	0.0010
4	56768	9	1.064	0.0010
5	34122	8	3.018	0.0118
6	7491	7	2.605	0.0102
7	8108	7	2.882	0.0113
8	4067	6	6.318	0.0987
9	1259	5	7.067	0.1104
10	1242	5	7.926	0.1238
11	523	4	11.889	0.7431
12	179	3	16.887	1.0548
13	130	3	11.474	0.7171
14	43	-	43.496	10.8741
15	17	-	16.748	4.1869
16	9	-	9.236	2.3090
			$\sum$	20.419

Table 1: Bit-allocation for the 16-band GG-scheme and a total rate of R_S=1.0 bpp.

3 Channel Error Effects

For joint source and channel coding, one must now consider, in addition to source coding or quantization errors, the effects of corrupted source bits, due to channel errors, on the reconstructed image. In particular, knowing the distribution parameters of the generalized Gaussian distribution associated with a particular subband i, denoted α_i and β_i, one can then evaluate the contribution to the overall mean-square reconstruction error due to an error in any given bit position. These contributions can be expressed in terms of individual bit sensitivities to errors in any given bit position and lead to a useful and tractable approximation to the combined effect of source and channel coding errors. To be sure, these bit sensitivities depend upon the particular coding scheme used to represent quantizer output levels or indices. In the work to be described here we do not seek

an optimum representation scheme as this depends rather explicitly upon the underlying source distribution as well as the detailed statistical description of the channel bit-error characteristics. Instead, we will be specifically concerned with the use of a sign-magnitude representation of quantizer output indices since it is uniformly applicable and leads to relatively robust performance. Indeed, we demonstrate that the sign-magnitude representation leads to lower bit-error sensitivities, and hence to improved performance, relative to either pure-magnitude or Gray-coded representations (see Section 3.2).

3.1 Effects of Channel Errors

Suppose that $\mathbf{P}_{i,l}$, $l = 0, 1, ..., (2^{n_i} - 1)$, represents the l^{th} error pattern associated with the transmission of data of class i (subband i) for $i = 1, 2, ..., K$. It is a binary[3] n_i-tuple with a 1 in those positions corresponding to an error and 0's elsewhere. For definiteness, for each i we take $\mathbf{P}_{i,0}$ to be the all-zero sequence corresponding to no channel errors.

The average error due to the combined effects of source and channel error effects associated with transmission of subband i data is then

$$\bar{e}_{i,n_i} = \sum_{l=0}^{2^{n_i}-1} e_{i,n_i}^{(l)} \Pr\{\mathbf{P}_{i,l}\} \ , \tag{15}$$

where $e_{i,n_i}^{(l)}$ is the conditional mse given that transmission error pattern $\mathbf{P}_{i,l}$ has occurred and $\Pr\{\mathbf{P}_{i,l}\}$ is the corresponding probability of this event. Corresponding to (11) for pure source coding, the combined distortion is then

$$\begin{aligned} D_{\text{s+c}} &= \sum_{i=1}^{K} \frac{s_i}{S} \cdot \bar{e}_{i,n_i} \\ &= \sum_{i=1}^{K} \frac{s_i}{S} \left(1 - \sum_{l=1}^{2^{n_i}-1} \Pr\{\mathbf{P}_{i,l}\} \right) e_{i,n_i} + \sum_{i=1}^{K} \frac{s_i}{S} \sum_{l=1}^{2^{n_i}-1} e_{i,n_i}^{(l)} \cdot \Pr\{\mathbf{P}_{i,l}\} \ , \end{aligned} \tag{16}$$

where we make use of the fact that $e_{i,n_i}^{(0)} = e_{i,n_i}$, the mse due solely to source coding effects. The first term then accounts for quantization error effects while the second term represents contributions due to both quantization and channel errors.

Assuming that all n_i positions of a codeword for the i^{th} subband data have the same probability of error p_i, we have

$$\Pr\{\mathbf{P}_{i,l}\} = p_i^{d_{i,l}} \cdot (1 - p_i)^{n_i - d_{i,l}} \ ; \ l = 0, 1, ..., 2^{n_i} - 1 \ , \tag{17}$$

[3] Recall that data from subband i is encoded using an n_i-bit quantizer

where $d_{i,l}$ is the Hamming weight of error pattern $\mathbf{P}_{i,l}$. More generally, assuming different probabilities of error $p_{i,j}$ for each of the n_i positions of a codeword for the i^{th} subband data, we have

$$\Pr\{\mathbf{P}_{i,l}\} = \prod_{j=1}^{n_i} p_{i,j}^{\psi_j(\mathbf{P}_{i,l})} \cdot [1 - p_{i,j}]^{1-\psi_j(\mathbf{P}_{i,l})} \ , \tag{18}$$

where

$$\psi_j(\mathbf{P}_{i,l}) = \begin{cases} 1 \ ; & \text{if the } j^{\text{th}} \text{ component of } \mathbf{P}_{i,l} \text{ is a 1} \\ 0 \ ; & \text{otherwise .} \end{cases} \tag{19}$$

In particular, the latter situation arises when unequal error protection is applied for different bit positions of n_i-bit codewords for subband i data.

By writing the conditional mse $e_{i,n_i}^{(l)}$ as the sum of the quantization error e_{i,n_i} and a term accounting for the effects due solely to transmission errors we have

$$e_{i,n_i}^{(l)} = e_{i,n_i} + A_{i,n_i}^{(l)} \ , \tag{20}$$

where $A_{i,n_i}^{(l)}$ denotes the bit-error sensitivity (additional mse) of a codeword of length n_i of subband i data, given the l^{th} error pattern. Using (16) and (20), the combined distortion due to source and channel coding can thus be written as

$$D_{\text{s+c}} = \sum_{i=1}^{K} \frac{s_i}{S} \cdot e_{i,n_i} + \sum_{i=1}^{K} \frac{s_i}{S} \sum_{l=1}^{2^{n_i}-1} A_{i,n_i}^{(l)} \cdot \Pr\{\mathbf{P}_{i,l}\} \ . \tag{21}$$

where the first term denotes the source coding (quantization) error D_s and the second term the additional mean-square error due to channel errors only.

We now approximate the additional distortion caused by error pattern $\mathbf{P}_{i,l}$ in terms of the single-bit-error sensitivities $A_{i,j}$, which account for the additional mse, given a single error in bit j, with $j = 1, 2, ..., n_i$ (i.e., the single-error patterns $\mathbf{P}_{i,l}$ with $l = 1, 2, 4, ..., 2^{(n_i-1)}$), of a codeword of subband i data as

$$A_{i,n_i}^{(l)} \lesssim \sum_{j=1}^{n_i} \psi_j(\mathbf{P}_{i,l}) \cdot A_{i,j} \ , \tag{22}$$

which is an upper bound for the case of multiple errors (i.e., $l \neq 1, 2, 4, 8, ..., 2^{(n_i-1)}$). Nevertheless, as the $p_{i,j}$ become small, the probability of multiple errors tend to be very small and thus the error terms for $l \neq 1, 2, 4, 8, ..., 2^{(n_i-1)}$ can be neglected, i.e., (22) holds with equality (single errors only). Finally, using (21) and (22), the overall distortion can be written as

$$\begin{aligned} D_{\text{s+c}} &\lesssim \sum_{i=1}^{K} \frac{s_i}{S} \cdot e_{i,n_i} + \sum_{i=1}^{K} \frac{s_i}{S} \sum_{l=1}^{2^{n_i}-1} \left(\sum_{j=1}^{n_i} \psi_j(\mathbf{P}_{i,l}) A_{i,j} \cdot \prod_{k=1}^{n_i} p_{i,k}^{\psi_k(\mathbf{P}_{i,l})} [1 - p_{i,k}]^{1-\psi_k(\mathbf{P}_{i,l})} \right) \\ &= \sum_{i=1}^{K} \frac{s_i}{S} \cdot e_{i,n_i} + \sum_{i=1}^{K} \frac{s_i}{S} \sum_{j=1}^{n_i} A_{i,j} \cdot p_{i,j} \ , \end{aligned} \tag{23}$$

where we have made use of the fact that

$$\sum_{l=1}^{2^{n_i}-1} \psi_j(\mathbf{P}_{i,l}) \cdot \prod_{k=1}^{n_i} p_{i,k}^{\psi_k(\mathbf{P}_{i,l})} [1-p_{i,k}]^{1-\psi_k(\mathbf{P}_{i,l})} = \mathrm{E}\{\psi_j(\mathbf{P}_{i,l})\}$$
$$= p_{i,j} \ , \qquad (24)$$

for any given $j \in 1, ..., n_i$.

3.2 Derivation of Bit-Sensitivities

The knowledge of the individual bit sensitivities $A_{i,j}$ is essential for the joint optimization of source and channel coding. In the following, the sensitivities will be derived for the general case of an n-bit quantizer for both the uniform threshold (UT) and the generalized Gaussian (GG) quantizer.

3.2.1 Scheme A: Uniform Threshold (UT) Quantizer

For this basic quantization scheme, when quantizing the quantization range $QR = [-\frac{Q}{2}; \frac{Q}{2}]$ with n bits, the sensitivity of the magnitude bits can be written as

$$A_{\mathrm{UT,m},j} = \left(2^j \cdot \frac{Q}{2^n}\right)^2 \quad ; \quad \text{for} \quad j = 0, ..., (n-2) \ , \qquad (25)$$

where $j = 0$ denotes the least significant bit (LSB) and $j = (n-2)$ denotes the most significant bit (MSB). The average sensitivity of the sign bit (SB) of the DC-band, which is modeled as a Gaussian distribution, is the summation over all possible corruptions (i.e., all possible magnitude values being corrupted to their negative values, resulting in twice the error of the actual magnitude) and can be written as

$$A_{\mathrm{UT,s,dc}} = \frac{Q^2}{2^{2n}} \sum_{k=1}^{2^{(n-1)}} (2k-1)^2 \cdot \left[\mathrm{erfc}\left(\frac{(k-1)Q/2^n}{\sqrt{2\sigma^2}}\right) - \mathrm{erfc}\left(\frac{k \cdot Q/2^n}{\sqrt{2\sigma^2}}\right)\right] \ . \qquad (26)$$

Similarly, the sensitivity of the sign bit of an AC-band can be expressed as (see Appendix B)

$$A_{\mathrm{UT,s,ac}} = \frac{Q^2}{2^{2n}} \cdot \sum_{k=1}^{2^{(n-1)}} (2k-1)^2 \cdot \left[\mathrm{P}\left(\frac{1}{\beta}, \left(\frac{k \cdot \frac{Q}{2^n}}{\alpha}\right)^\beta\right) - \mathrm{P}\left(\frac{1}{\beta}, \left(\frac{(k-1) \cdot \frac{Q}{2^n}}{\alpha}\right)^\beta\right)\right] \ , \qquad (27)$$

with $\mathrm{P}(a,x)$ again the incomplete Gamma function. To obtain the final effect of a bit error in one sample on the reconstructed image, one has to normalize the sensitivities $A_{i,j}$ of the samples to the image by multiplying with the factor s_i/S, as done in (23).

3.2.2 Scheme B: Optimum (nonuniform) Generalized Gaussian (GG) Quantizer

Similarly, the sensitivity for the nonuniform quantizer based on the generalized Gaussian distribution, which is applied to the AC-bands only, can be derived. Let's denote $d(x_{l,a}, x_{l,b})$ as the distance between the reconstruction levels $x_{l,a}$ and $x_{l,b}$, where, due to symmetry, we refer to the positive range only (i.e., mean = 0, $0 \leq x_l \leq \infty$, $a, b \in (0, ..., (2^{n-1} - 1))$). The probability, that a sample to be quantized falls into the interval $[x_{t,k}, x_{t,k+1}]$ with $k \in (0, ..., (2^{n-1} - 1))$ is $\Pr(x_{l,k}) = 1/2 \cdot (\mathrm{P}(1/\beta, x_{t,k+1}) - \mathrm{P}(1/\beta, x_{t,k}))$. So the sensitivity for the $(n-1)$ magnitude bits can be expressed as (see Appendix B)

$$A_{\mathrm{GG,m},j} = 2 \cdot \sum_{l=0}^{2^j-1} \sum_{k=0}^{(2^{n-2-j}-1)} [\Pr(x_{l,a}) + \Pr(x_{l,b})] \cdot d^2(x_{l,a}, x_{l,b}) \quad ; \quad \text{for} \quad j = 0, ..., (n-2) \ , \tag{28}$$

with

$$a = l + k \cdot 2^{(j+1)} \quad \text{and} \quad b = l + k \cdot 2^{(j+1)} + 2^j \ , \tag{29}$$

where again $j = 0$ denotes the LSB and $j = (n-2)$ denotes the MSB. The sensitivity of the sign bit can be derived in a similar way as

$$A_{\mathrm{GG,s}} = 2 \sum_{k=0}^{2^{(n-1)}-1} \Pr(x_{l,k}) \cdot (2x_{l,k})^2 \ , \tag{30}$$

with $x_{l,k}$ the quantization level of interval k.

To demonstrate the close correspondence between analytical and simulated bit-sensitivities, both for the UT- and GG- quantizer, we plotted both results in Fig. 2 for a representative bit allocation at a rate $R_{\mathrm{S}} = 1.0$ bpp for the well-known LENNA image (see Table 1). The bit-allocation assigned the optimum number of quantization bits n_i to the different subbands, in order to obtain the minimum distortion (from eqn. 11) for the given (maximum) source rate (from eqn. 12). As can be seen, the DC-subband (denoted by $i = 1$) and the lower-frequency AC-subbands were assigned a higher number of quantization bits, whereas the high-frequency AC-subbands were assigned only a few bits or even none. To have a better view of the wide range of the $A_{i,j}$, we plotted $\log_{10}(A_{i,j})$ versus the subband i. The precise estimation of the bit-sensitivities, together with the analysis of the quantization error, is the basis for the later joint source-channel bit-allocation. One can also note in Fig. 3, which shows the simulated sensitivities for alternative representation schemes (which again could very precisely be predicted), that this way of coding (sign-magnitude) results in lower bit-sensitivities compared to pure magnitude or Gray coding of the samples (especially the first two sensitivities of each subband). Although there exist optimum representation strategies to minimize

sensitivities for a given source distribution, for simplicity, we restrict ourselves to sign-magnitude coding.

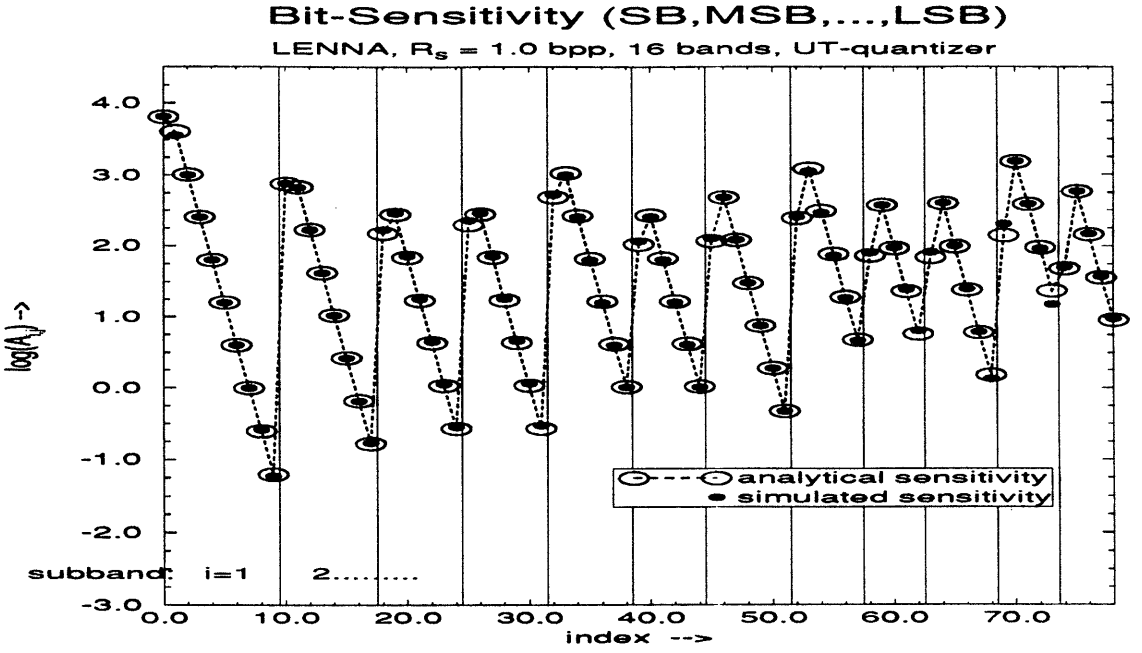

a.) UT-quantizer, subband i=1,...,12

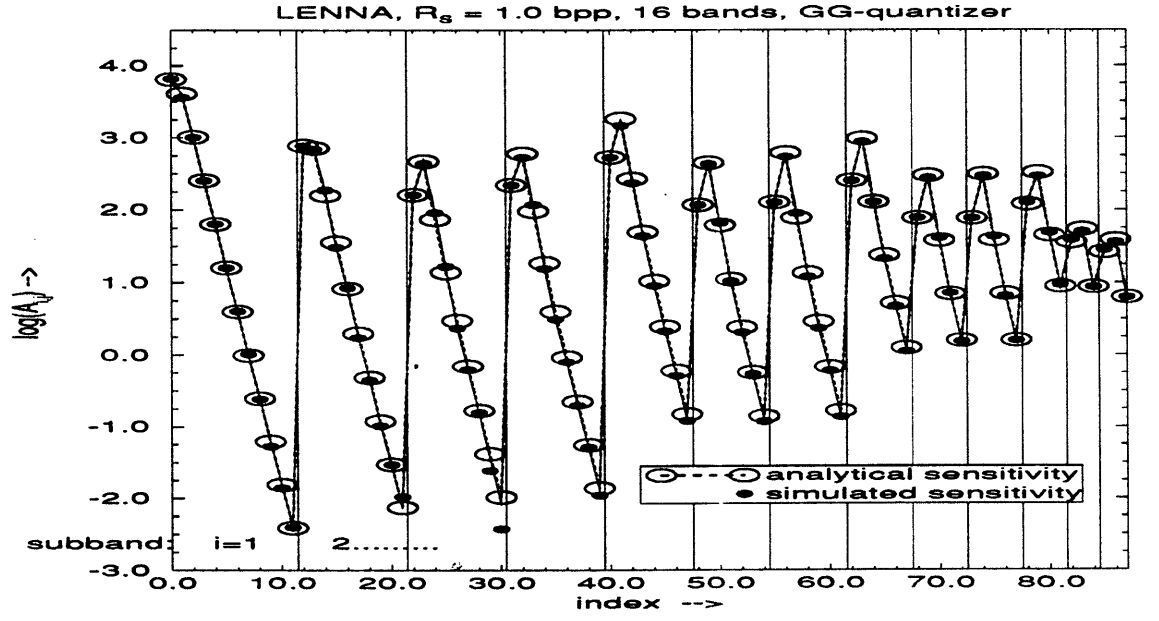

b.) GG-quantizer, subband i=1,...,13

Figure 2: Comparison of analytical and simulated bit-sensitivities, SB, MSB,....,LSB.

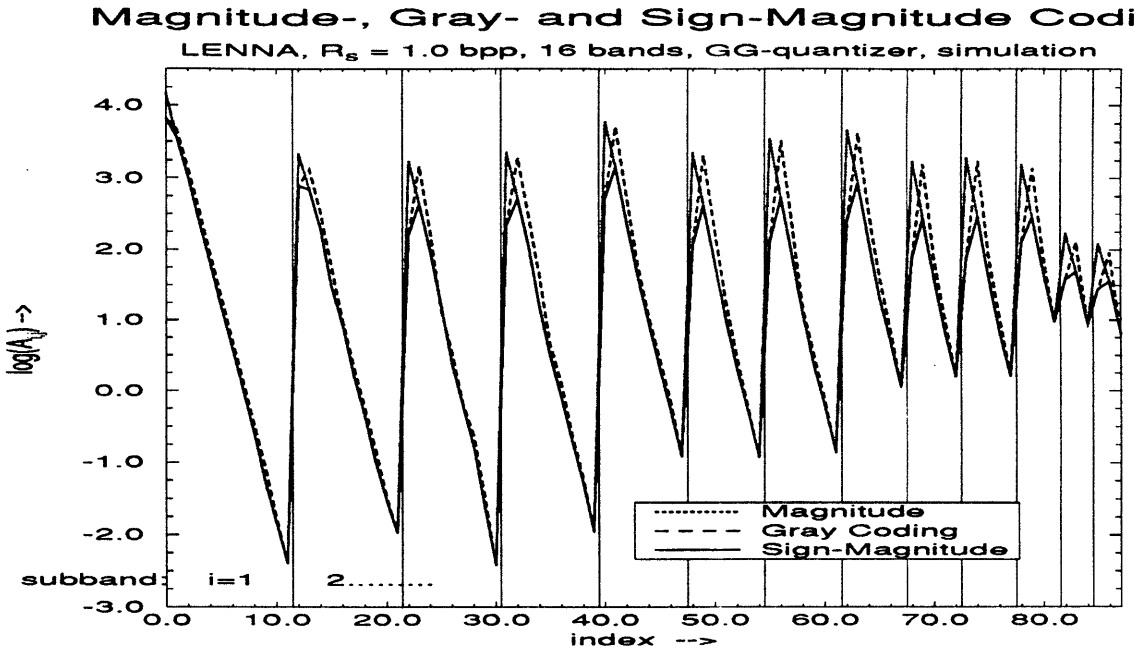

Figure 3: Comparison of bit sensitivities for magnitude, Gray and sign-magnitude coding of subband samples.

3.3 Channel Coding

For a real-world system with different sensitivities $A_{i,j}$, we allocate different channel code rates to the different encoder output components, giving us different levels of protection (i.e., bit-error rates). One can either allocate one single channel code rate, resulting in identical bit-error probabilities p_i for all bits of a codeword of subband i data, or one could allocate different channel code rates, resulting in bit-error probability $p_{i,j}$ for the j^{th} bit, $j = 1, 2, ..., n_i$ of a sample within subband i. In particular, this requires a class of codes that allow different rates. We chose the binary rate-compatible punctured convolutional (RCPC) codes with memory $\nu = 6$, because they allow convenient implementation of all codes of different rates within this class without changing the encoder or decoder by simply varying the number of punctured bits. Furthermore, they allow very precise prediction of the expected bit-error rate (BER) for specified channel conditions and a given channel code rate. The reader is referred to the original paper [14] for a performance evaluation in an additive white Gaussian noise (AWGN) and a Rayleigh fading environment. When calculating the expected bit-error probabilities for the different code-rates R_f, one has to deal with the loose behaviour of the transfer-function upper bound for low signal-to-noise ratios. Since the bit-allocation algorithm always considers the uncoded BER with code rate R_f=1 first, any discrepancy in BER for $R_f \neq 1$ due to looseness of the upper bounds is avoided by choosing the smaller of

the computed bound and the uncoded bit-error probability. Furthermore, it should be emphasized that, although one could apply other families of channel codes, we restricted attention to binary codes, which allow a reasonably accurate analysis of BER versus signal-to-noise ratio E_s/N_0 to obtain an overall analysis of the combined source and channel coding.

By denoting as $R_{i,j}$ the channel code rate (in bits per channel use) assigned to position j of the i^{th} subband, we can write the average channel code rate (in source bits per channel use) of subband i as

$$R_{\text{C},i} = \frac{n_i}{\sum_{j=1}^{n_i} 1/R_{i,j}} \; . \tag{31}$$

The overall average channel code rate (in source bits per channel use) can then be written as

$$R_{\text{C}} = \frac{\sum_{i=1}^{K} n_i \cdot s_i}{\sum_{i=1}^{K} [(n_i \cdot s_i)/R_{\text{C},i}]} = \frac{\sum_{i=1}^{K} n_i \cdot s_i}{\sum_{i=1}^{K} s_i \cdot \sum_{j=1}^{n_i} (1/R_{i,j})} \; . \tag{32}$$

4 Rate-Distortion Behavior

4.1 Overall Rate and Distortion

Being able to calculate the distortion introduced by source coding (eqn. 11) and the overall distortion including the (remaining) channel errors (eqn. 23) (i.e., the sum of the source coding distortion D_{S} and the distortion due to transmission errors D_{C}), one can rewrite the overall distortion $D_{\text{S+C}}$ (in mse) for every possible assignment of different quantization bits per subband n_i and different channel code rates $R_{i,j}$ for the n_i different positions of the samples of subband i (with a resulting BER $p_{i,j}$) as

$$D_{\text{S+C}} = D_{\text{S}} + D_{\text{C}} = \sum_{i=1}^{K} D_{\text{S+C},i} = \sum_{i=1}^{K} \frac{s_i}{S} \cdot \left(e_{i,n_i} + \sum_{j=1}^{n_i} A_{i,j} \cdot p_{i,j} \right) \; . \tag{33}$$

The resulting overall rate $R_{\text{S+C}} = R_{\text{S}}/R_{\text{C}}$ (in channel uses per pixel) can be written as

$$R_{\text{S+C}} = \frac{1}{S} \sum_{i=1}^{K} s_i \cdot \sum_{j=1}^{n_i} \frac{1}{R_{i,j}} = \frac{1}{S} \sum_{i=1}^{K} \frac{n_i \cdot s_i}{R_{\text{C},i}} = \frac{1}{S} \sum_{i=1}^{K} s_i \cdot R_{\text{S+C},i} \; . \tag{34}$$

The problem is then, similarly to the bit-allocation problem for pure source coding, to find the number of quantization bits n_i for every subband i together with the channel code rates $R_{i,j}$ for the different classes of sensitivities to obtain a minimum overall distortion $D_{\text{S+C}}$ under the constraint of a given maximum overall rate $R_{\text{S+C}}$. It is also possible to solve this problem to match a specified overall distortion $D_{\text{S+C}}$ with the minimum overall rate $R_{\text{S+C}}$.

4.2 Joint Source and Channel Bit Allocation

The task is to allocate the bits corresponding to a certain overall rate R_{S+C} in a way, that we obtain the minimum distortion for a certain (uncoded) bit-error rate or E_s/N_0 on the channel. Therefore, we can apply the same optimal bit-allocation algorithm of Westerink et al. [13] to the different subbands, knowing their overall rate-distortion behavior $D(R)$ in exactly the same way as described previously for pure source coding. To calculate the overall distortion (mse) corresponding to a certain rate (c.u. per pixel), we start with the following approach.

4.2.1 No Code-Allocation within a Subband

For the first step in evaluating the final rate-distortion behaviour, we restrict attention to a single channel code per subband. This means every bit of the quantized samples within subband i has the same channel code with the resulting bit-error probability p_i, i.e., $R_{i,j} = R_{C,i}$ for $j = 1, ..., n_i$. Therefore, we applied the following procedure for every subband i: We first calculated the joint source and channel distortion depending on the rate $D_{S+C,i}(R_{S+C,i})$. Taking a look at Fig. 4, one can see, we started with the case of no source coding at all ($n_i = 0$), resulting in the distortion $D_{S+C,i} = D_{S,i}(n_i = 0) = (1/S)\sum_{m=1}^{s_i} y_{i,m}^2$, the weighted variance of subband i, with $y_{i,m}$ the m^{th} sample of subband i. We then quantize with $n_i = 1$ bit and we assign all possible F channel code rates R_f, with $f = 0, 1, ..., F$ (with $f = 0$ as no channel coding, $f = 1$ as the weakest code with the highest code rate and $f = F$ the best available protection with the lowest code rate) to this $n_i = 1$ source bit and, using (33), we calculate the joint distortion. This procedure is repeated after incrementing the number of quantization bits n_i until one reaches a sufficiently low joint distortion within the subband i. This procedure can be seen in Fig. 4, where we plotted the joint distortion (as $\log_{10}$(mse) for a better representation of the wide range of values) versus the overall rate (in c.u. per pixel) for subband $i = 3$ at an $E_s/N_0 = 0$ dB which corresponds to an uncoded BER of $p = 0.0786$ with available channel code rates of 1/1, 8/9, 4/5, 2/3, 4/7, 1/2, 4/9, 4/10, 4/11, 1/3, 4/13, 4/15, 1/4. One can see the decreasing distortion with the increase of quantization bits. The decrease in distortion due to more and more channel coding saturates at a distortion equal to the quantization noise (when quantizing with n_i bits). This is why there is a 6 dB difference of the (horizontal) saturation lines corresponding to each increment in quantization bits. In Fig 4, we also plotted the final operational joint rate-distortion function as

the convex hull for this particular subband[4]. This will be used in the following joint bit-allocation procedure, together with corresponding operational R-D-functions (that show a similar behavior) for all the K subbands.

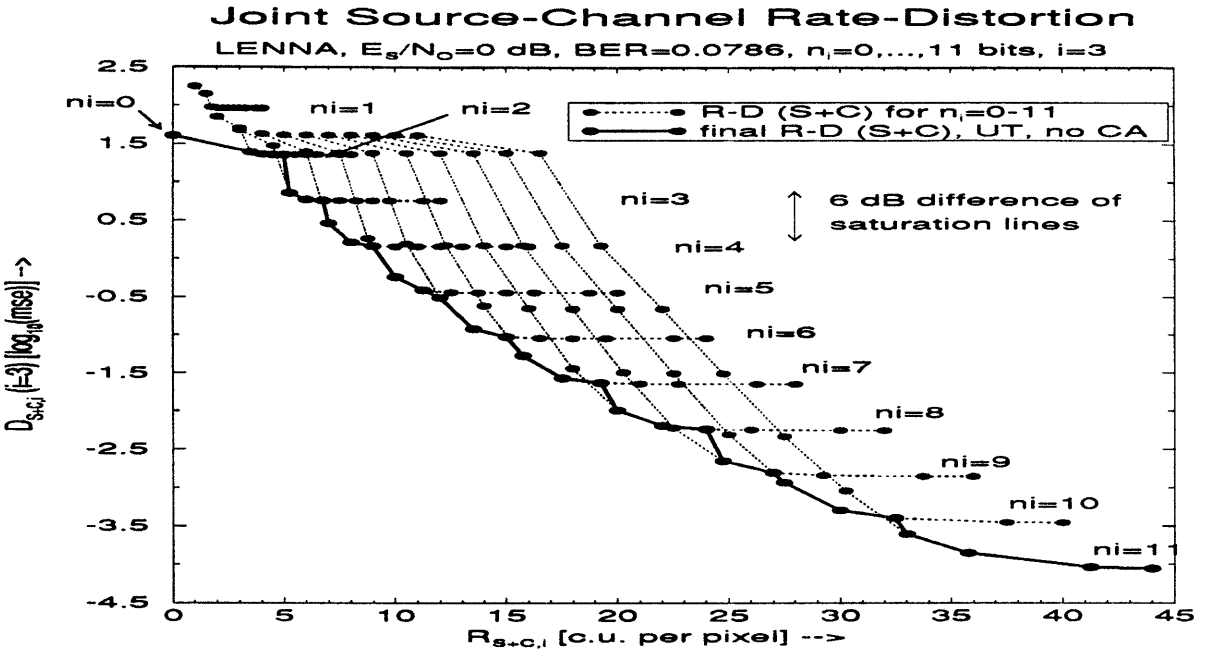

Figure 4: Overall rate-distortion behavior of joint source and channel coding, applied to subband i=3, **no** code-allocation, UT-quantizer.

4.2.2 Code-Allocation within a Subband

To improve the overall performance, one can perform a code-allocation (CA) within every subband. This means, that the n_i different source bits of subband i can receive different protection (according to their needs). This seems logical, since the source bits cover a wide range of sensitivities (see Fig. 2), and it obviously is a waste of resource (redundancy) if we do not make use of some form of unequal error protection (UEP). The calculation of the operational R-D-functions of the different subbands is then altered in the following way. After assigning a specific number of quantization bits n_i one has to perform code-allocation procedures before incrementing n_i. The code-allocation is done for average channel rates ranging from $\bar{R}_{\min} = 1.0$, which means every source bit has no channel coding, to $\bar{R}_{\max} = R_{f=F}$, which means every source bit obtains maximum protection. An average channel code rate $\bar{R}$ with $\bar{R}_{\min} < \bar{R} < \bar{R}_{\max}$ means the available redundancy is

[4]Note that in this case ($i = 3$), all possible distortions for $n_i = 1$ are greater than the variance ($n_i = 0$) and thus are not considered when evaluating the operational joint rate-distortion function.

allocated in an optimum way to the different sensitivities (different code rates to the different sensitive bits, UEP) as to minimize the channel distortion $D_{c,i}(n_i)$. We plotted this procedure for the same conditions as above in Fig. 5a, where one can see, as a result of the performed code-allocation, the much smoother and steeper behavior of the corresponding R-D-function (compared to Fig. 4), which means increased performance and more variety for the later joint source-channel bit-allocation to choose from.

To show the benefits of this code-allocation procedure and the better source coding performance of the GG-quantizer, we plotted the final R-D-functions (the same conditions apply as before) for the UT- and GG-quantizer in Fig. 5b. As one can see, the performance improves when using CA for the UT instead of none. Furthermore, using the GG-quantizer increases the performance even more. Furthermore, to dramatically enhance the performance of the source coder, similarly to [15], we partitioned every subband into fields with size equal to that of the low-frequency subband ($i = 1$). Since different fields of one subband represent different regions of the image, depending on the image content they may have very different statistical properties. This gives the joint bit-allocation a much wider variety of choices for allocating bits (i.e., local adaptivity). So, for the remainder, we consider K=16 subbands after the wavelet transform, partitioned into $\tilde{K}$=1024 fields, and for the source-channel coding, we use the GG-quantizer with CA.

4.3 Simulation Results

Having the operational R-D-functions, the joint bit-allocation based on [13] assigns bits to the bands, in order to obtain the minimum overall distortion for a given overall rate R_{s+c} for a specific channel signal-to-noise ratio. Contrary to [3], where we used a two-stage algorithm for the bit-allocation, to allocate the channel bits after the source bits, and then searched for the optimum source-to-channel rate ratio, here we jointly allocate source and channel bits in a single bit-allocation. The analytical overall performance is shown in Fig. 6a, where we plotted the R-D-diagrams of the 1024 field-GG scheme for different E_s/N_0 on an AWGN channel. One can see the typical R-D-behavior including the improved performance (lower distortion) with increasing signal-to-noise ratio. We also included some simulation results with the LENNA image, being actually source and channel encoded, transmitted and decoded (with some remaining channel errors) 50 times. This was done for the overall rates R_{s+c}=0.5, 0.75 and 1.0 bpp and an E_s/N_0=0, 2 and 4 dB, using the $\nu = 6$ RCPC codes. The exact values of simulation and analysis can be found in Table 2. The side information to be transmitted, which comprises the statistical properties of the

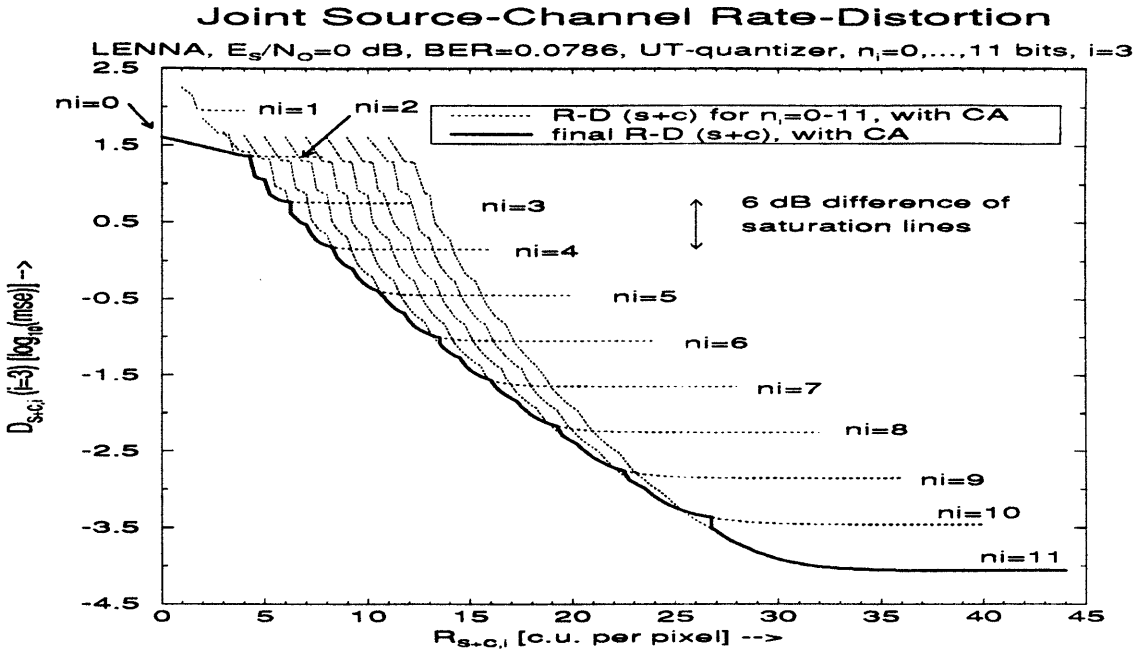

a.) **with** code-allocation, UT-quantizer

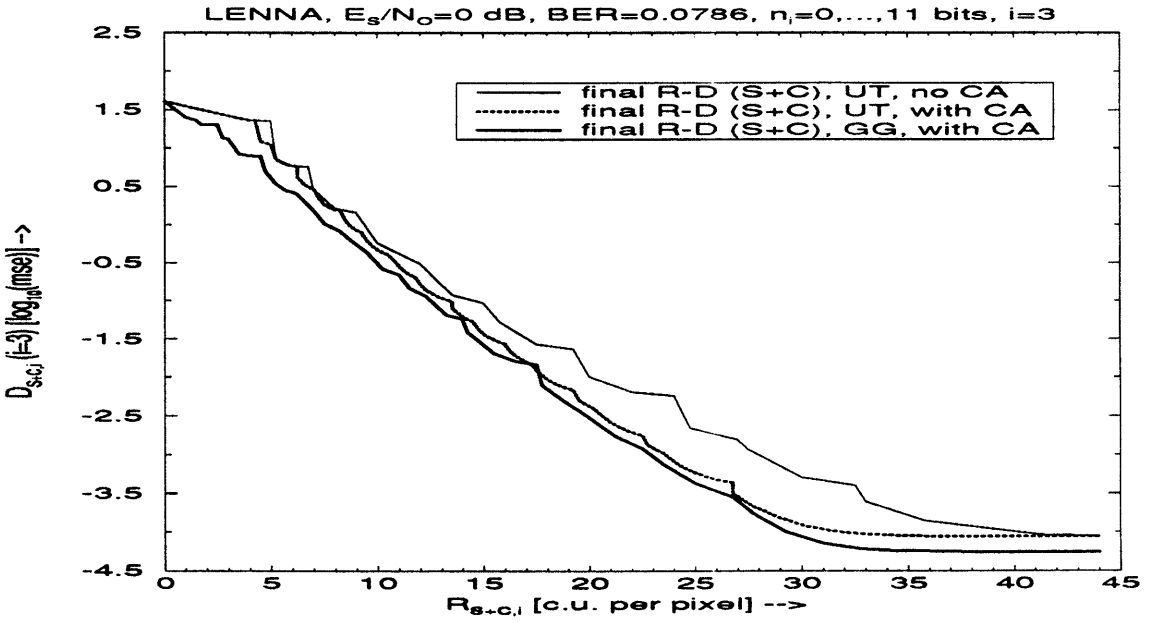

b.) Comparison of R-D-diagrams for UT- and GG-quantizer

Figure 5: Overall rate-distortion behavior of joint source and channel coding, applied to subband i=3.

coded image, accounts for less than 5 % of the actual data and thus is neglected. One can note the very close correspondence of analytical and simulated performance that results from the precise analysis of quantization error, bit-sensitivities and bit-error rates.

In Fig. 6b, we compare the joint R-D-behavior of three different schemes (with CA), namely the 16 band-UT, the 1024 field-UT and the 1024 field-GG scheme for an E_s/N_0=0 dB. One can

E_s/N_0 [dB] (BER uncod.)	R_{s+c} [c.u./ pixel]	D_S [mse]		D_C [mse]		D_{s+c} [mse]		D_{s+c} [PSNR]	
		analyt.	simul.	analyt.	simul.	analyt.	simul.	analyt.	simul.
0 dB	0.5	42.42	43.15	4.26	4.67	46.68	47.82	31.44	31.34
	0.75	27.56	28.27	3.06	3.09	30.62	31.37	33.27	33.17
$(7.9 \cdot 10^{-2})$	1.0	19.81	20.30	2.46	2.40	22.26	22.70	34.66	34.57
2 dB	0.5	32.93	33.42	3.31	3.41	36.24	36.83	32.54	32.47
	0.75	20.85	21.28	2.25	2.24	23.11	23.53	34.49	34.42
$(3.8 \cdot 10^{-2})$	1.0	14.89	15.29	1.56	1.49	16.45	16.78	35.97	35.88
4 dB	0.5	26.41	26.98	1.86	2.89	28.28	29.87	33.62	33.38
	0.75	16.31	16.60	1.37	2.05	17.68	18.65	35.66	35.43
$(1.3 \cdot 10^{-2})$	1.0	11.57	11.83	0.94	1.33	12.51	13.16	37.16	36.94

Table 2: Performance of joint source channel coding for code memory $\nu = 6$.

see the improvement as one moves to more and more sophisticated schemes. Note that these overall operational R-D-functions can be calculated, for every source-channel coding scheme, once a specific channel code family is chosen (with the knowledge of the associated BER-performance) and provided that there exists an analysis of source coding error and of the sensitivity to channel errors.

We also illustrated in Fig. 7 some representative images, which were transmitted over an AWGN-channel at a signal-to-noise ratio of E_S/N_0=0 dB and an overall rate of R_{s+c}=1.0 bpp. One can get a very good indication of the improvements if one compares the images, beginning from an unprotected image with no transmission error (a), to an unprotected image with channel errors (b), on to the various schemes with increasing performance (16-UT (c), 1024-UT (d) and 1024-GG (e)) and, finally, comparing them to the result of a transmitted image at the channel capacity (f). The same results for E_S/N_0=2 dB and R_{s+c}=0.5 bpp can be seen in Fig. 8. Both figures show the large amount of distortion due to channel errors in the unprotected images (b). The jointly optimized images of the 16-UT (c) scheme look much better, but still the images indicate the effects of the quantization error due to the suboptimum source coding performance. With better source coding (1024-UT (d)), we increase the quality of the image, but there is some distortion noticeable. The best results can be obtained with the 1024-GG scheme (e), which combines sharpness with less annoying noise. The best theoretical quality, assuming the 1024-GG scheme, but no channel errors when transmitting at the channel capacity (f), shows only minor improvements in the case of E_S/N_0=2 dB and R_{s+c}=0.5 bpp (Fig. 8) and almost no improvement in the case of E_S/N_0=0 dB and R_{s+c}=1.0 bpp (Fig. 7). The coding results (PSNR and R_S) of the images can be seen in

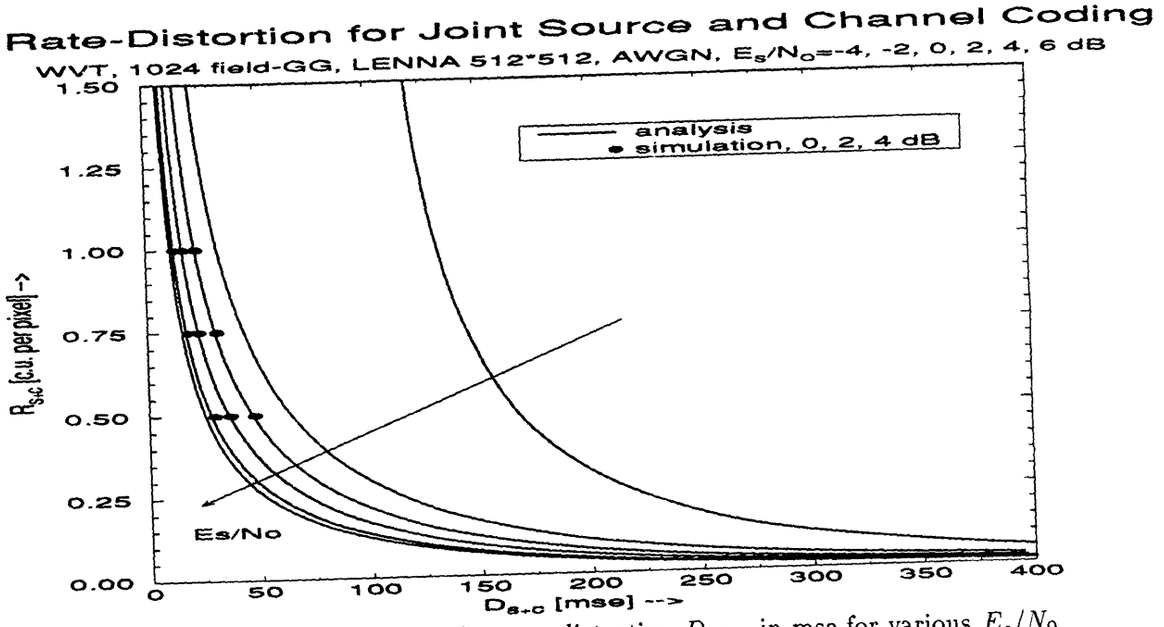

a.) Rate R_{S+C} in c.u. per pixel versus distortion D_{S+C} in mse for various E_s/N_0

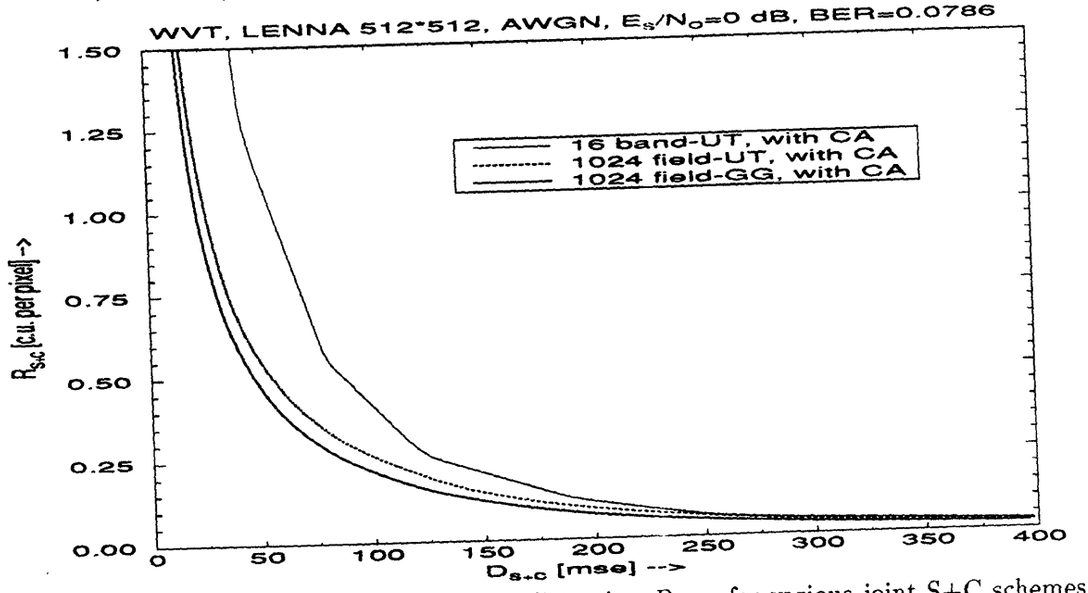

b.) Rate R_{S+C} in c.u. per pixel versus distortion D_{S+C} for various joint S+C schemes

Figure 6: Overall rate-distortion behavior of joint source and channel coding.

Table 3.

5 Theoretical Performance Bounds

We are now interested in obtaining theoretical bounds on the R-D behavior of combined source-channel coding approaches which will prove useful in assessing the relative efficiency of different real-world schemes, such as the approach described here. In fact, we will develop a sequence

a.) Source coding only, BER=0.0

b.) Source coding only, BER=0.079

c.) UT-16, $R_s = 0.48$ bpp

d.) UT-1024, $R_s = 0.56$ bpp

e.) GG-1024, R_s=0.57 bpp

f.) GG-1024 at capacity, R_s=0.60 bpp

Figure 7: Simulation results for $R_{s+c} = 1.0$ bpp and E_S/N_0=0 dB.

a.) Source coding only, BER=0.0

b.) Source coding only, BER=0.038

c.) UT-16, $R_s = 0.35$ bpp

d.) UT-1024, $R_s = 0.35$ bpp

e.) GG-1024, R_s=0.36 bpp

f.) GG-1024 at capacity, R_s=0.38 bpp

Figure 8: Simulation results for $R_{s+c} = 0.5$ bpp and E_S/N_0=2 dB.

Joint Source-Channel Coding Scheme	E_S/N_0=0 dB - BER=0.079 R_{S+C}=1.0 bpp		E_S/N_0=2 dB - BER=0.038 R_{S+C}=0.5 bpp	
	R_S	PSNR	R_S	PSNR
no trans. errors	1.00	38.175	0.50	34.480
unprotected	1.00	16.040	0.50	18.224
16 - UT	0.48	29.683	0.35	29.489
1024 - UT	0.56	33.766	0.35	31.765
1024 - GG	0.57	34.594	0.36	32.477
Capacity	0.60	35.470	0.38	33.201

Table 3: Simulation results of the images depicted in Fig.'s 9 and 10.

of such bounds predicting successively improved performance but implying increasing levels of system complexity. These bounds will be useful in assessing additional performance/complexity tradeoffs above and beyond the specific combined source-channel coding approach considered here and provide the basis for potential further improvement.

As a first step, assume that it is possible to transmit at the channel cutoff rate R_0, in bits/c.u., and that this results in negligibly small bit-error rate. The cutoff rate is generally accepted as the largest signaling rate *practically* achievable for which arbitrarily small bit-error probability can be expected [16]. This information-theoretic bound is said to be *practically* achievable in the sense that in many real-world situations it's possible to design specific channel coding schemes requiring only reasonable decoder complexity and yet demonstrating performance approaching theoretical predictions based upon cutoff rate considerations. This assumption then allows us to assess the additional improvement in R-D performance possible if the binary RCPC codes were replaced by more powerful, yet practically implementable, binary channel coding schemes. The cutoff rate for binary antipodal signalling on the AWGN channel is given by [16], [17]

$$R_0 = \log_2\left(\frac{2}{1+e^{-E_s/N_0}}\right) \; ; \qquad \text{bits/c.u.} \tag{35}$$

The first information-theoretic performance bound will then be obtained under the assumption of equal error protection (EEP) at the largest practical signalling rate for all bits of all subbands[5], i.e., we assume $R_{C,i} = R_0$, $i = 1, 2, ..., K$, and that this assignment results in zero channel errors. The resulting performance bound, illustrated in Fig. 9b for subband $i = 3$ and in Fig. 10 for overall system performance, provides only marginal improvement over the best of our real-world coding results (e.g., 1024 field-GG, with CA). This is due to the fact that, although the operational R-D

[5]This is stronger than the no CA case considered previously in that now all subbands are assumed coded identically but result in zero channel errors.

functions of selected subbands (e.g., $i = 3$) show considerable improvements for very low distortions (i.e., $\log_{10}(\text{mse}) < 0$), as illustrated in Fig. 9b, the joint source-channel coding allocation algorithm results in distortion allocations for these subbands at higher levels (i.e., $\log_{10}(\text{mse}) > 0$) where the performance improvement is rather small. This would indicate that with EEP schemes, it's difficult to improve much on the practical approach described here, even with the use of more powerful binary channel codes.

As a second, improved bound we consider the case where limited CA is now allowed within each subband. More specially, we consider either[6] no channel coding with $R_{i,j} = 1$ or channel coding with $R_{i,j} = R_0$ for the different coded bits of each subband (field). In the former case, the bit-error probability is taken as the raw symbol-error probability, while it is assumed zero for the latter. We make use of the same optimization strategy as employed in Section 4.2.2 to assign the $R_{i,j} \in \{1, R_0\}$. This approach allows more flexibility in tailoring the degree of coding to the sensitivities of the individual bits in an effort to minimize the overall distortion subject to a total transmitted rate constraint. Furthermore, even though it has the same R-D performance as the case where all bits are coded at the cutoff rate ($R_{\text{C},i} = R_0$), it provides a higher degree of freedom in choosing distortions (rates) for the following bit-allocation process. Indeed, a similar analysis of our previous example (subband $i = 3$, E_s/N_0=0dB) exhibits a steeper behavior than the optimized RCPC coding approach as illustrated in Fig. 9a,b. For the overall R-D performance, the resulting bound is only marginally improved over the case with EEP ($R_{\text{C},i} = R_0$) at the channel cutoff rate as illustrated in Fig. 10 (e.g., 1024 field-GG, $R_{i,j} = 1||R_0$). Nevertheless, this case ($R_{i,j} = 1||R_0$) does have some advantages since it assigns just the right amount of protection to the coded bits and, due to wider selection of possible distortions (or rates), the bit-allocation can be more efficient.

The preceding two bounds are representative of *practically* achievable performance with real-world systems provided we use state-of-the-art channel coding of reasonable complexity and restrict attention to fixed-level quantizers for each subband (field). We now consider the potential performance achievable if some form of variable-length entropy coding of the (optimum) GG-quantizer output indices is employed to further reduce the source coding rate for a given level of distortion. More specifically, the first-order entropy of individual subbands (fields), when quantizing with n_i bits, is

[6]This case is referred to as $1||R_0$ in what follows.

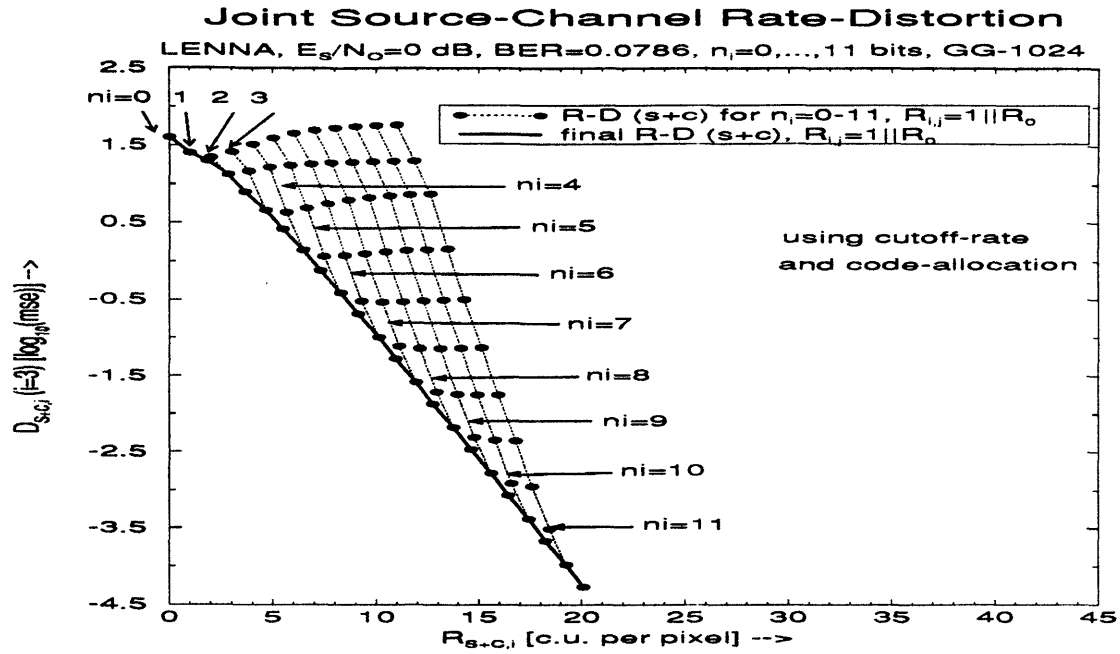

a.) Rate $R_{\mathrm{S+C},i}$ in c.u. per pixel versus distortion $D_{\mathrm{S+C},i}$ in mse for subband i=3

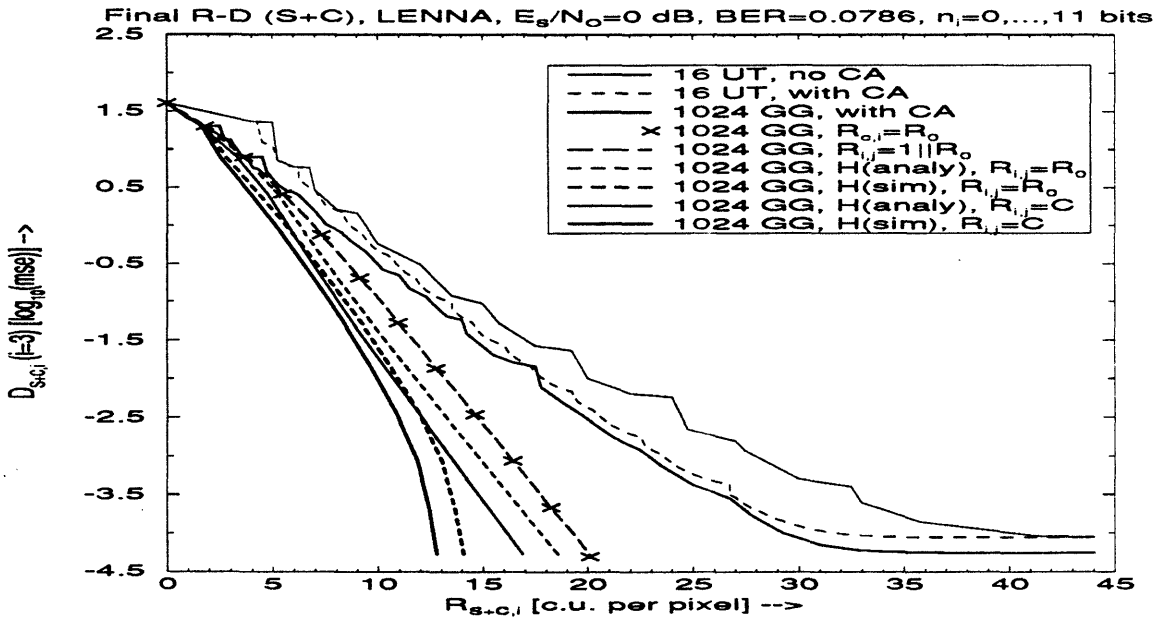

b.) Rate $R_{\mathrm{S+C},i}$ versus distortion $D_{\mathrm{S+C},i}$ for various joint S+C schemes, subband i=3

Figure 9: Rate-distortion behavior of joint source and channel coding for subband i=3.

$$H(y;n_i) = -\sum_{k=1}^{2^{n_i}} p(y_k)\cdot\log_2 p(y_k)\ ; \quad \text{bits/sample}\ , \tag{36}$$

where y_k, $k = 1,2,...,2^{n_i}$, represent quantizer indices and $p(y_k)$ is the corresponding probability. The operational R-D functions for each subband (field) are then modified by assuming the source coding rate (in bits/sample) is measured as the corresponding first-order index entropy. Note that

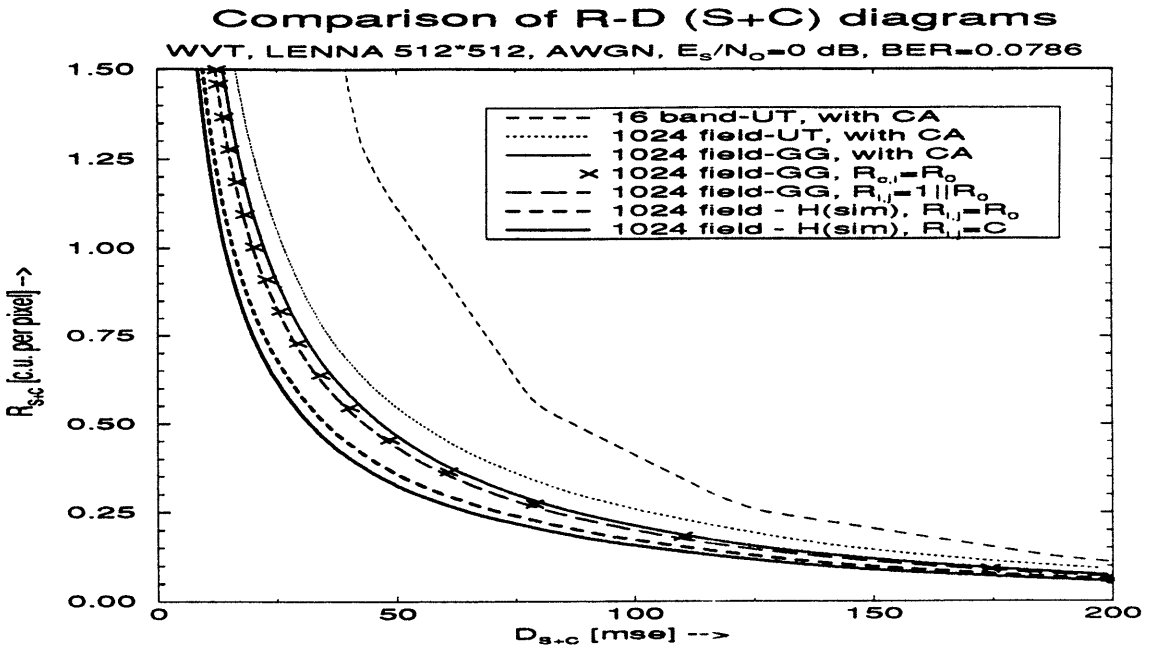

Figure 10: Comparison of overall rate-distortion behavior of joint source and channel coding for various schemes.

in order to achieve this performance some form of variable-rate entropy coding will be required which is extremely sensitive to channel errors, and associated error propagation effects, if there are no other precautions taken such as providing periodic embedded synchronization marks. Since the differential effects of individual channel errors on these practical variable-length coding schemes is difficult to analyze, we will restrict attention to EEP schemes. In particular, we will develop additional information-theoretic bounds by assuming EEP channel coding operation at either the cutoff rate ($R_{i,j} = R_0$) or the channel capacity ($R_{i,j} = C$); in either case, we assume zero bit-error probability. The first of these bounds ($R_{i,j} = R_0$) provides a useful bound on *practically* achievable performance while the second ($R_{i,j} = C$) provides a bound on *theoretically* achievable performance and is useful in assessing absolute performance limitations. We should note at this time that these same assumptions will lead to even improved R-D bounds if entropy-constrained quantizer (ECQ) design approaches were employed rather than simply entropy coding the level-constrained quantizer (LCQ) designs as used here. This is considered outside the scope of the present investigation.

The resulting performance bounds for these two cases is illustrated in Fig. 9b for subband $i = 3$, and in Fig. 10 for the overall R-D performance. In Fig. 9b, we illustrate results for both analytical evaluation of the entropy under the GG assumption as well as use of simulated performance. The difference between the simulated and analytically derived entropy results are due to at least two reasons. First, there is some statistical variability in the simulated results due to the relatively small

number of samples per subband[7] (field) $s_i = 256$. Secondly, there is some modeling mismatch under the GG assumption which results in some inaccuracies in the analytical results. Consequently, we expect that the actual R-D performance is somewhere in between those two results. It follows then from Fig. 9b that these entropy-derived bounds demonstrate some additional potential for performance improvement by use of more efficient source coding (e.g., entropy coding of quantizer indices) provided we are willing to accept the increased complexity associated with the variable-length entropy coding. Furthermore, it should be noted from Fig. 9b that the potential performance improvement for subband $i = 3$ is substantial only at very low distortions[8]. Since the combined source-channel coding allocation scheme typically allocates a range of rates and/or distortions to the various subbands, the overall R-D performance is a weighted average over these individual subband allocations. The resulting overall R-D performance, as illustrated in Fig. 10, indicates that the entropy-derived bounds are only marginally better than the fixed-level information-theoretic bounds which are in turn quite close to the achievable performance with our proposed combined source-channel coding approach.

Some final comments on the results in Fig. 10 are in order. These results, including the information-theoretic bounds, although useful, apply only to the specific wavelet-based encoding scheme here and for the fixed image LENNA. Nevertheless, subject to these qualifications, the results are useful in comparing different combined source-channel coding strategies and in relating their performance to theoretical limits. In particular, they demonstrate the excellent behavior of the best of our UEP strategies (1024 field-GG, with CA) which is readily implemented using existing source/channel coding techniques. Furthermore, the results indicate that only marginal performance improvements can be expected using more powerful channel codes (i.e., R_0 or $1||R_0$ level-constrained bounds) or more complex entropy coding of quantizer indices (i.e., R_0 or C entropy-derived bounds). Clearly, additional work using a wider range of source material is required to firmly establish the efficacy and robustness of the proposed procedure.

6 Summary and Conclusions

In this paper we described a methodology for evaluating the rate-distortion behavior of combined source and channel coding approaches. We applied this evaluation procedure to the quantization

[7] For $i = 1, 2, 3, 4$ the number of samples per subband and per field are the same since they are of size of the DC-subband.

[8] The R-D behavior of the entropy-derived bounds, particularly for $R_{i,j} = C$, appear non-convex in the logarithmic scale although the actual behavior is, in fact, convex-cup on a linear scale.

of images with an encoder using a discrete wavelet transform. In order to derive the dependence of rate and distortion for a combined source and channel coding scheme, we calculated the effects of channel errors, the bit-error sensitivities to the reconstructed image, both for a uniform threshold (UT) quantizer and an optimum nonuniform quantizer, based on the generalized Gaussian (GG) distribution. We showed how to perform an optimum bit-allocation procedure, where the bits were jointly allocated to source and channel coding in one operation. Considerably better performance of the jointly optimized scheme employing the GG-quantizer (making use of local adaptivity) under noisy channel conditions (additive white Gaussian noise) was shown. Furthermore, we compared the performance to theoretical performance bounds and we showed that the real-world system closely approaches the rate-distortion behavior of our system operating at the (theoretical) cutoff rate. Other theoretical limits based on the channel capacity and the real source entropy are much harder to approach. Simulation results demonstrate the very close correspondence of theory and the actual system performance and also show the improvements and the benefits that can be realized by using a combined source and channel coding scheme.

Although our results are derived for BPSK signalling in AWGN, there are still ways to improve the overall performance of a source-channel system by using higher-order modulation schemes (i.e., QPSK, 16 QAM etc.) or combined modulation and channel coding schemes (coded modulation, multi-resolution modulation), especially when the channel bit-error rate is not as high as in our examples. One can also develop both practical and theoretical limits for these techniques and determine the proper modulation scheme for the best overall efficiency. The evaluation of the combined source and channel performance can also be performed for other channels, and especially for the Rayleigh fading channel we would expect to see even higher performance gains of the proposed methods compared to uncoded transmission.

APPENDIX A

Optimum (nonuniform) Quantization Levels for the Generalized Gaussian Distribution

For $N = 2^n$ the number of quantization levels and n the number of quantization bits, the limits of the quantization range can be estimated for a linear distortion measure ($\theta = 1$) or a square distortion measure, i.e., the mse ($\theta = 2$), using Roe's formula [11], by

$$\int_0^{x_k} p(t)^{\frac{1}{1+\theta}} \mathrm{d}t = 2C_1 k + C_2 \quad ; \text{with} \quad p(t) = \kappa \cdot \mathrm{e}^{-\left(\frac{t}{\alpha}\right)^{\beta}} \quad \text{and} \quad \kappa = \frac{\beta}{2\alpha\Gamma(1/\beta)}. \qquad (\mathrm{A}-1)$$

To calculate C_1 and C_2, we set $x_k = \infty$ $(k = N)$, substitute with $y = (\frac{t}{\alpha})^{\beta} \cdot \frac{1}{1+\theta}$ and obtain

$$\int_0^{\infty} \kappa^{\frac{1}{1+\theta}} \cdot e^{\left(-(\frac{t}{\alpha})^{\beta} \cdot (\frac{1}{1+\theta})\right)} \mathrm{d}t = \kappa^{\frac{1}{1+\theta}} \cdot \frac{\alpha}{\beta}(1+\theta)^{1/\beta} \int_0^{\infty} y^{(\frac{1}{\beta}-1)} e^{-y} \mathrm{d}y \ . \qquad (A-2)$$

Using the Gamma-function $\Gamma(z)$, (A-2) can be written as

$$\kappa^{\frac{1}{1+\theta}} \cdot \frac{\alpha}{\beta}(1+\theta)^{1/\beta}\Gamma(1/\beta) = R \ . \qquad (A-3)$$

Due to symmetry, for $k = 0$ $(x_k = -\infty)$, (A-1) becomes $-R$, so one obtains

$$C_2 = -R \quad ; \text{for} \quad k = 0 \ , \qquad (A-4)$$

and with (A-4),(A-1) and setting $k = N$, which results in $C_1 = R/N$, (A-1) becomes

$$2C_1 k + C_2 = R\left(\frac{2k}{N} - 1\right) \ . \qquad (A-5)$$

For $x_k \geq 0$, with the same substitution we obtain

$$\int_0^{\infty} \kappa^{\frac{1}{1+\theta}} \cdot e^{\left(-(\frac{t}{\alpha})^{\beta} \cdot (\frac{1}{1+\theta})\right)} = \kappa^{\frac{1}{1+\theta}} \cdot \frac{\alpha}{\beta}(1+\theta)^{1/\beta} \int_0^{y(x_k)} y^{(\frac{1}{\beta}-1)} e^{-y} \mathrm{d}y \ , \qquad (A-6)$$

with

$$y(x_k) = \left(\frac{x_k}{\alpha}\right)^{\beta} \cdot \frac{1}{1+\theta} \ . \qquad (A-7)$$

Using the incomplete Gamma-function $\mathrm{P}(a, x)$

$$\mathrm{P}(1/\beta, x) = \frac{1}{\Gamma(1/\beta)} \int_0^{x} e^{-x} \cdot x^{(\frac{1}{\beta}-1)} \mathrm{d}x \ , \qquad (A-8)$$

(A-2) can be written as

$$\kappa^{\frac{1}{1+\theta}} \cdot \frac{\alpha}{\beta}(1+\theta)^{1/\beta} \cdot \Gamma(1/\beta) \cdot \mathrm{P}\left(1/\beta, \ \frac{1}{1+\theta}\left(\frac{x_k}{\alpha}\right)^{\beta}\right) = R\left(\frac{2k}{N} - 1\right) \ . \qquad (A-9)$$

Using (A-3) and (A-9), we obtain

$$\mathrm{P}\left(1/\beta, \ \frac{1}{1+\theta}\left(\frac{x_k}{\alpha}\right)^{\beta}\right) = \left(\frac{2k}{N} - 1\right) = S \quad ; \text{for} \quad x_k \geq 0 \ . \qquad (A-10)$$

To prevent the limits of the quantization thresholds ($k = 0$ and $k = \infty$) to be identical with $\pm\infty$ of the distribution, we introduce a correction term κ_θ, which results in

$$S_t = \frac{2k - N}{N + \kappa_\theta} \quad ; \text{for} \quad \frac{N}{2} \leq k \leq N \ , \qquad (A-11)$$

for the quantization thresholds, and

$$S_l = \frac{2k + 1 - N}{N + \kappa_\theta} \quad ; \text{for} \quad \frac{N}{2} \leq k < N \ , \qquad (A-12)$$

for the reconstruction levels. So finally, using the inverse function of the incomplete Gamma-function $\mathrm{P}^{-1}(1/\beta, y)$, with (A-10) and (A-11) we obtain for the quantization thresholds

$$x_{t,k} = \left[(1+\theta)\,\mathrm{P}^{-1}\left(\frac{1}{\beta}, \frac{2k-N}{N+\kappa_\theta}\right)\right]^{1/\beta} \cdot \alpha \quad ; \text{for} \quad \frac{N}{2} \le k \le N\,, \tag{A-13}$$

and for the reconstruction levels

$$x_{l,k} = \left[(1+\theta)\,\mathrm{P}^{-1}\left(\frac{1}{\beta}, \frac{2k+1-N}{N+\kappa_\theta}\right)\right]^{1/\beta} \cdot \alpha \quad ; \text{for} \quad \frac{N}{2} \le k < N\,. \tag{A-14}$$

Using symmetry, one obtains the values for $0 \le k < \frac{N}{2}$ as $x_{t,k} = -x_{t,(N-k)}$ and similarly as $x_{l,k} = -x_{l,(N-1-k)}$.

The correction term κ_θ will be calculated under the assumption that for $N = 2$ levels, the reconstruction levels $x_{l,0}$ and $x_{l,1}$ will be the the first absolute moment of the distribution. This assumption also provides a good matching of the formulas for small N. The first absolute moment (due to symmetry) can be written as

$$x_a = 2\int_0^\infty t \cdot p(t)\mathrm{d}t = 2\int_0^\infty t \cdot \frac{\beta}{2\alpha\Gamma(1/\beta)} \mathrm{e}^{-\left(\frac{t}{\alpha}\right)^\beta} \mathrm{d}t\,, \tag{A-15}$$

and using the substitution $x = (t/\alpha)^\beta$ one can easily obtain

$$x_a = \frac{\alpha \cdot \Gamma(2/\beta)}{\Gamma(1/\beta)}\,. \tag{A-16}$$

So, for the case $N = 2$ and especially $k = 1$, one can write using (A-14) and (A-16)

$$x_{l,1} = \left[(1+\theta)\,\mathrm{P}^{-1}\left(\frac{1}{\beta}, \frac{1}{2+\kappa_\theta}\right)\right]^{1/\beta} \cdot \alpha = \frac{\alpha \cdot \Gamma(2/\beta)}{\Gamma(1/\beta)}\,, \tag{A-17}$$

which results in the solution for the correction term

$$\kappa_\theta = \left[\mathrm{P}\left(1/\beta, \left(\frac{\Gamma(2/\beta)^\beta}{\Gamma(1/\beta)} \cdot \frac{1}{1+\theta}\right)\right)\right]^{-1} - 2\,. \tag{A-18}$$

APPENDIX B

Derivation of Bit-Sensitivities

Scheme A: UT

The average sensitivity of the sign bit of an AC-band is the weighted summation over all possible corruptions (i.e., all possible values being corrupted to their negative values, resulting in twice the error of the actual value) and can be written as

$$A_{\mathrm{UT,s,ac}} = \sum_{k=1}^{2^{(n-1)}} \mathrm{pr}_k \cdot \left[(2k-1) \cdot \frac{Q}{2^n}\right]^2\,, \tag{B-1}$$

with n the number of quantization bits, $QR = [-\frac{Q}{2}; \frac{Q}{2}]$ the overall quantization range and pr_k the probability of samples x to be coded as amplitude k. This probability can be expressed as

$$\begin{aligned} \mathrm{pr}_k &= \Pr\left\{x \in \left[(k-1)\frac{Q}{2^n}, k\frac{Q}{2^n}\right]\right\} \\ &= \int_{(k-1)\frac{Q}{2^n}}^{k\frac{Q}{2^n}} \frac{\beta}{2\alpha\Gamma(1/\beta)} \cdot \mathrm{e}^{(x/\alpha)^\beta} \\ &= \frac{1}{2} \cdot \left[\mathrm{P}\left(\frac{1}{\beta}, \left(\frac{k \cdot \frac{Q}{2^n}}{\alpha}\right)^\beta\right) - \mathrm{P}\left(\frac{1}{\beta}, \left(\frac{(k-1) \cdot \frac{Q}{2^n}}{\alpha}\right)^\beta\right)\right] . \end{aligned} \tag{B-2}$$

So considering that due to symmetry the probability doubles, and by using (B-1) and (B-2), one obtains

$$A_{\mathrm{UT,s,ac}} = \frac{Q^2}{2^{2n}} \cdot \sum_{k=1}^{2^{(n-1)}} (2k-1)^2 \cdot \left[\mathrm{P}\left(\frac{1}{\beta}, \left(\frac{k \cdot \frac{Q}{2^n}}{\alpha}\right)^\beta\right) - \mathrm{P}\left(\frac{1}{\beta}, \left(\frac{(k-1) \cdot \frac{Q}{2^n}}{\alpha}\right)^\beta\right)\right] . \tag{B-3}$$

Scheme B: GG

For the bit sensitivities of the magnitude bits of the non-equidistant quantizer based on the generalized Gaussian distribution, we have to take a closer look at the error, that occurs, if a bit is corrupted. All the possible pairs of reconstruction levels $(x_{l,a}, x_{l,b})$ on the positive half of the distribution, that go with a bit corruption of bit j with $j = 0, ..., (n-2)$, where $j = 0$ denotes the LSB and $j = (n-2)$ denotes the MSB, can be described as

$$\left(l + (k \cdot 2^{j+1}), \quad l + (k \cdot 2^{j+1}) + 2^j\right) \quad ; \text{for} \quad l = 0, ..., (2^j - 1) \quad \text{and} \quad k = 0, ..., (2^{n-2-j} - 1) . \tag{B-4}$$

So one has to sum twice (symmetry) over all these possible pairs $(x_{l,a}, x_{l,b})$, weight the associated errors $d^2(x_{l,a}, x_{l,b})$ with the probabilities $\Pr\{x_{l,a}\}$ and $\Pr\{x_{l,b}\}$ and one obtains

$$A_{\mathrm{GG,m},j} = 2 \cdot \sum_{l=0}^{2^j-1} \sum_{k=0}^{(2^{n-2-j}-1)} [\Pr\{x_{l,a}\} + \Pr\{x_{l,b}\}] \cdot d^2(x_{l,a}, x_{l,b}) \quad ; \text{for} \quad j = 0, ..., (n-2) . \tag{B-5}$$

References

[1] J. W. Modestino and D. G. Daut, "Combined source-channel coding of images," *IEEE Trans. Commun.*, vol. COM-27, pp. 1644–1659, Nov. 1979.

[2] J. W. Modestino, D. G. Daut, and A. L. Vickers, "Combined source-channel coding of images using the block cosine transform," *IEEE Trans. Commun.*, vol. COM-29, pp. 1261–1274, Sep. 1981.

[3] M. J. Ruf and P. Filip, "Joint source and channel coding applied to the pyramid vector quantizer," in *Proc. IEEE IT Symposium, San Antonio*, p. 391, 1993.

[4] N. Tanabe and N. Farvardin, "Subband image coding using entropy-coded quantization over noisy channels," *IEEE Journal of Selected Areas in Com*, vol. 10, pp. 926–943, June 1992.

[5] M. J. Ruf, "On channel coding for image transmission," in *Proc. 6th Joint Conference on Communications and Coding, Selva, Italy*, 1994.

[6] J. Hagenauer, "Source-controlled channel decoding," *accepted for publ. in IEEE Trans. Comm.*, 1995.

[7] Joint Photographic Experts Group, *JPEG Technical Specification, Revision 5*, January 1990.

[8] J. W. Woods and S. D. O'Neil, "Subband coding of images," *IEEE Trans. ASSP*, vol. 34, pp. 1278–1288, Oct. 1986.

[9] S. G. Mallat, "A theory for multiresolution signal decomposition: the wavelet representation," *IEEE Trans. Pattern Anal. Machine Intell.*, vol. PAMI-11, pp. 674–693, July 1989.

[10] J. D. Johnston, "A filter family designed for use in quadrature mirror filter banks," in *Proc. IEEE ICASSP*, pp. 291–294, 1980.

[11] G.M.Roe, "Quantizing for minimum distortion," *IEEE Trans. IT*, vol. 10, pp. 384–385, Oct. 1964.

[12] P. Filip, "Compander quantizer," *personel communication*, 1993.

[13] P. H. Westerink, J. Biemond, and D. E. Boekee, "An optimal bit allocation algorithm for sub-band coding," in *Proc. IEEE ICASSP*, pp. 757–760, 1988.

[14] J. Hagenauer, "Rate-compatible punctured convolutional codes (RCPC codes) and their applications," *IEEE Trans. Commun.*, vol. COM-36, pp. 389–400, Apr. 1988.

[15] M. J. Ruf, "A high performance fixed rate compression scheme for still image transmission," in *Proceedings DCC '94, Data Compression Conference*, IEEE Computer Society Press, 1994.

[16] J. L. Massey, "Coding and modulation in digital communications," in *Proc. Int. Zurich Seminar on Digital Communications*, (Zurich, Switzerland), pp. E2(1)–E2(4), 1974.

[17] J. M. Wozencraft and I. M. Jacobs, *Principles of Communication Engineering*. New York: Wiley, 1965.